Molecular Imaging of Retinal Gliosis in Transgenic Mice Induced by Kainic Acid Neurotoxicity

Gideon Ho,[1,2] *Saravana Kumar,*[1,2] *Xiao Shan Min,*[1,3] *Yin Ling Kng,*[1] *Ming Yang Loh,*[1] *Shujun Gao,*[1] *and Lang Zhuo*[1]

Purpose. Gliosis is a universal response of the central nervous system to diverse insults. Here the authors aimed to develop a noninvasive fluorescence system to monitor and quantify retinal gliosis in real time.

Methods. Transgenic mice expressing green fluorescent protein (GFP) under the control of the glial fibrillary acidic protein promoter were treated with excitatory neurotoxicant kainic acid (KA) through a single intraperitoneal injection to induce gliosis in the brain and the retina. The expression of the GFAP-GFP transgene as a surrogate reporter for gliosis was noninvasively and longitudinally imaged with a confocal scanning laser ophthalmoscope for 2 weeks to monitor the progression of gliosis.

Results. The authors demonstrated that KA-induced gliosis (an elevation in GFP fluorescence intensity [FI]) could be noninvasively detected starting on day 3 and that it peaked on day 7, as quantified for the optic disc astrocytes. A significant increase in the FI in retinal glial cells was also visible on the processed images. Immunohistochemistry in defined regions of the brain (hippocampal CA1, CA3, dentate gyrus) known to be affected by KA neurotoxicity showed that severe gliosis in these regions occurred at day 7, when retinal gliosis peaked.

Conclusions. The current real-time fluorescent imaging method described here is a powerful preclinical tool to directly monitor retinal gliosis caused by various retinopathies. In addition, this molecular imaging method should be useful in assessing retinal neurotoxicity and in therapeutic development in a preclinical setting. (*Invest Ophthalmol Vis Sci.* 2009;50: 2459–2464) DOI:10.1167/iovs.08-2133

Various ophthalmic conditions and numerous systemic diseases outside the eye can cause retinopathy, a noninflammatory degenerative disease of the retina that leads to visual field loss or blindness. Many of the retinal disorders can be diagnosed with the aid of retinal and optic nerve examination. Examples of such disorders include hypertension,[1–3] congenital heart disease,[4] neurofibromatosis,[5–7] diabetes,[8–10] liver disease,[11,12] eye diseases such as age-related macular degeneration[13] and glaucoma,[14] and neurodegenerative disease.[15,16] All these earlier reports highlighted the importance and value of eye examination in disease diagnosis by association in human patients. However, for ethical reasons, causative studies and compound screening with ocular imaging cannot be conducted in humans. Methods for in vivo imaging of the retina have traditionally been structurally based using reflection imaging or contrast-injected fluorescence angiography,[17,18] ultrasound, or optical coherent tomography. However, these anatomically based ocular imaging methods do not allow real-time collection of signal transduction at the molecular level. Furthermore, potential scarring, leakage, and inflammatory reaction in the eye that were incurred by the injection of contrast agents could compromise the intended experimental readouts.[19]

Astrocytes and Müller cells are the major glial cell types in the retina[20] and express a basal level of glial fibrillary acidic protein (GFAP) under normal circumstances. However, retinal glia respond to diseases or insults by increasing GFAP production[21] through hypertrophy, hyperplasia, or both. Previous studies have shown that GFAP can be used as a biomarker to study retinopathies in fixed tissues or live tissues ex vivo.[16,22–24] Based on early observations, we proposed that the real-time reporter GFP (green fluorescent protein), when coupled to a GFAP promoter, should serve as an effective optical surrogate probe for noninvasively detecting and monitoring retinopathies in living mouse models given that the eye is transparent to optical signals. In the present study, we used the excitatory neurotoxicant kainic acid (KA) and optic nerve transection to establish proof-of-concept.

Methods

Transgenic GFAP-GFP Mice

Generation and genotyping of the transgenic GFAP-GFP mice were performed as previously described.[25] Adult mice (8–10 weeks old) in the FVB/N background were used. Animal husbandry was provided by Biological Resource Center (Biopolis, Singapore). The experimental protocol covering the present study was approved by the Institutional Animal Care and Use Committee and was conducted in compliance with the ARVO Statement for the Use of Animals in Ophthalmic and Vision Research.

Neurotoxicant and Dosing

KA was purchased from Sigma-Aldrich (K0250; St. Louis, MO). Each of the five mice in the treatment group received a single intraperitoneal injection of KA (25 mg/kg in saline). An equal number of mice injected with saline served as controls. Initial retinal imaging was performed immediately before dosing, and subsequent imaging was performed 3, 7, and 14 days after dosing.

Optic Nerve Transection

Optic nerve transection (OT) was performed unilaterally on the right eyes of four mice. Each mouse was anesthetized by a single intraperi-

From the [1]Institute of Bioengineering and Nanotechnology, Singapore.

[2]These authors contributed equally to the work presented here and should therefore be regarded as equivalent authors.

[3]Present affiliation: Department of Ophthalmology, XiangYa Hospital, South Central University, Changsha, Hunan, People's Republic of China.

Supported by the Institute of Bioengineering and Nanotechnology (IBN) and the Biomedical Research Council (BMRC) for the Agency of Science, Technology and Research (A*STAR), Singapore.

Submitted for publication April 7, 2008; revised September 20, October 27, and December 4 and 25, 2008; accepted March 20, 2009.

Disclosure: **G. Ho**, None; **S. Kumar**, None; **X.S. Min**, None; **Y.L. Kng**, None; **M.Y. Loh**, None; **S. Gao**, None; **L. Zhuo**, None

The publication costs of this article were defrayed in part by page charge payment. This article must therefore be marked "*advertisement*" in accordance with 18 U.S.C. §1734 solely to indicate this fact.

Corresponding author: Lang Zhuo, Institute of Bioengineering and Nanotechnology, 31 Biopolis Way, The Nanos, 04–01, Singapore 138669; lzhuo@ibn.a-star.edu.sg.

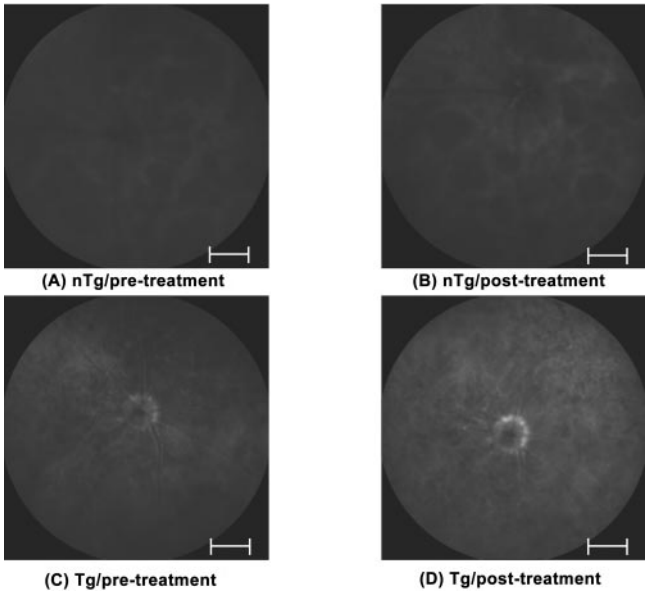

FIGURE 1. Composite fluorescent retinal images before and after KA treatment. Each composite image was formed by direct frame averaging of 55 raw images using the computing software. Only images for the left eye (OS) are shown here. KA treatment did not significantly induce autofluorescence in the retina or optic disc, as seen in the images from a nontransgenic (nTg) mouse before (**A**) or 1 week after (**B**) KA treatment. On the other hand, KA treatment caused a specific and significant increase in GFP fluorescence in the optic disc and the retina, when compared with an image from a transgenic (Tg) mouse before (**C**) or 1 week after (**D**) KA treatment. All the mice used in this section were 8-week-old males of FVB/N background. Scale bar, 250 μm.

toneal injection of tribromoethanol (Avertin; Sigma-Aldrich) at a dose of 0.15 mL/10 g body weight. Under an operating light microscope, the conjunctiva was incised, and the muscles and connective tissues were separated to expose the intraorbital optic nerve. The optic nerve was then transected approximately 2 mm behind the globe, with care taken to avoid injury to the central retinal artery. The retina was then examined ophthalmoscopically to ensure that the integrity of blood vessels was preserved. To avoid infection, antibiotics were administered intraperitoneally and topically on both eyes for 3 days after the operation. Each left eye was maintained as the control in all four mice.

Preparation of Mice

Each mouse was anesthetized by a single intraperitoneal injection of tribromoethanol (Avertin; Sigma-Aldrich) at a dose of 0.15 mL/10g body weight, and the pupils were dilated with a drop of 0.5% sterile ophthalmic solution (cyclopentolate hydrochloride; Cyclogyl; Alcon, Puurs, Belgium). Custom-made polymethylmethacrylate hard contact lenses (Cantor & Nissel, Northamptonshire, UK) were used to mount the mouse eyes to collect spherical optical aberration and to minimize dehydration of the cornea during imaging. For consistency, the lack of corneal or lens opacity was confirmed by an eye specialist before retinal imaging.

Scanning Laser Ophthalmoscope Imaging

The second version of the Heidelberg scanning laser ophthalmoscope (Heidelberg Retina Angiograph [HRA II]; Heidelberg Engineering, Dossenheim, Germany) modified with a 55° external wide-angle objective lens was used for the current mouse retinal imaging work. The 55° lens reduces the laser beam diameter to 1.7 mm, thus allowing more light to couple onto the mouse retina. Several studies using various scanning laser ophthalmoscopes for imaging in rats[23,26–28] and mice[29,30] have been published, with the latest studies on mice[31,32] using the first version of the HRA (or HRA I). To image GFP in the retinal glia, a 488-nm argon laser and a barrier filter (>500 nm) were used to acquire a stack of images at a frequency of 5 Hz from the nerve fiber layer (NFL). For each eye, 45 individual raw images were continuously collected using a fixed x-y-z setting on the HRA II in a time-frame of approximately 9 seconds. Because of the involuntary movements (breathing and heartbeat) of the anesthetized mouse, individual raw images acquired from the same eye using a fixed dial (x-y-z) could actually represent a series of consecutive images in transition. Therefore, the processing of individual raw images into a final composite figure is needed for image presentation and signal quantification.

Retinal Image Processing and Signal Quantification

To achieve a superior signal-to-noise and a resolution on the final composite images, we developed a novel and fully automated image processing algorithm based on averaging through a pixel rank matching criterion. This proposed algorithm consists of four major components: detecting landmark points, establishing point-to-point correspondence, aligning images by affine transformation, and aligning images through the novel rank-matching technique. The full development of the algorithm is described in a separate article.[33] All image processing and signal quantification in the present study were per-

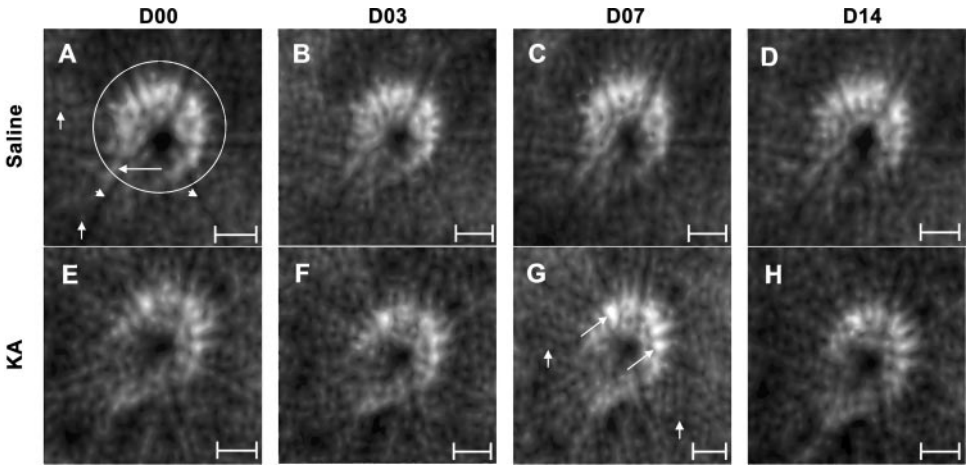

FIGURE 2. Representative noninvasive longitudinal retinal imaging of transgenic GFAP-GFP mice (saline vs. KA). Eight-week-old male transgenic mice injected with saline or KA were subject to retinal imaging on 0, 3, 7, and 14 days after injection. Each composite image was assembled using our algorithm from a total of 45 raw images acquired at the NFL. As illustrated (**A**), most of the FI was from the astrocytes within the optic disc (*circle*). Retinal blood vessels (*arrowheads*), associated retinal glial cells in the optic disc (*long arrow*), and surrounding region (*short arrows*) were all visible at the NFL. This pattern stayed fairly constant from day 0 to day 14 in the saline group (**A–D**). However, in the KA group (**E–H**), an increase in FI was observed in the retinal glial cells (*long arrows*) within the optic disc on day 7 (**G**). In addition, FI and the number for glial cells (*short arrows*) labeled by GFP in the surrounding retina were also significantly elevated on day 7 (**G**). The increase in FI on day 7 seemed to subside by day 14 (**H**). Scale bars, 100 μm.

formed with this algorithm unless otherwise indicated. In the present study, only fluorescence intensity (FI) from the astrocytes within the optic disc was used for quantification. Each astrocyte or cluster of astrocytes has a localized profile and a distinct peak FI, which is the averaged peak FI value over all astrocytes and astrocyte clusters in the optic disc region. Peak FIs of these astrocytes were determined through an image processing routine known as extended maxima transform. Quantified values were expressed as mean ± SEM and were statistically tested using Friedman nonparametric comparison on repeated FI measures.

Immunohistochemistry of Retinal Wholemounts and Brain Sections

Seven days after dosing, the mice were humanely killed and perfused with 50 mL of 1× PBS (pH 7.4) and an equal volume of ice-cold 4% paraformaldehyde (PFA; in 1× PBS, pH 7.4) before tissue harvest. For retinal wholemount, the eyes were further fixed in 4% PFA overnight at 4°C. They were dissected at the equator, and the lens and vitreous were removed. The retina was then dissected free from the choroid and sclera and mounted on a glass slide for subsequent immunohistochemistry (IHC).

For frozen tissue sectioning, the brains were fixed in 4% PFA for 4 hours at 4°C and were soaked in 30% sucrose at 4°C overnight. Processed tissues were embedded in OCT freezing medium for subsequent sectioning on a cryostat (CM-3050S; Leica Microsystems, Nussloch GmbH, Nussloch, Germany). For IHC, coronal cryosections (5 μm) of the CA1, CA3, and dentate gyrus of the hippocampus (bregma, −1.94 mm; interaural, 1.86 mm) according to the atlas of the mouse brain,[34] together with retina wholemounts, were stained with anti-GFAP polyclonal antibody raised in rabbit (Z0334; Dako, Carpinteria, CA) in 1:200 dilution overnight at 4°C. The bound primary antibody on the tissues was detected with a secondary antibody conjugated to Texas Red (Ab7088; Abcam, Cambridge, MA) in 1:100 dilution at room temperature for 2 hours. After mounting in mounting medium (Vectashield, H1000; Vector Laboratories, Inc., Burlingame, CA), the stained tissues were examined on a confocal microscope (LSM 510 META; Carl Zeiss Microimaging GmbH, Jena, Germany).

Results

Imaging and Image Processing for Quantification of Retinal Gliosis Induced by KA

The original (raw) images obtained from the retinas of transgenic GFAP-GFP mice had a high signal-to-noise ratio compared with the synthetic fluorescent dyes (FITC and ICG) commonly used in retinal angiography,[31] which made quantitative analysis of the transgene expression difficult. To enhance the signal-to-noise ratio, a stack of raw images can be processed with the built-in software in the HRA II set or with the direct frame averaging module in the computing software (MatLab; MathWorks, Natick, MA) to obtain reasonably good composite images at a low magnification (Fig. 1). It was clear at this magnification that the transgenic (Tg) retina from the KA-treated mouse (Fig. 1D) had a significantly higher FI over the saline control (Fig. 1C). It was also reassuring that the nontransgenic (nTg) retina from the saline-treated mouse (Fig. 1A) or with KA (Fig. 1B) yielded minimum and comparable fluorescence in the optic disc and the surrounding retina. However, at a higher magnification, we found that the quality of the composite images processed by the HRA II built-in software or the com-

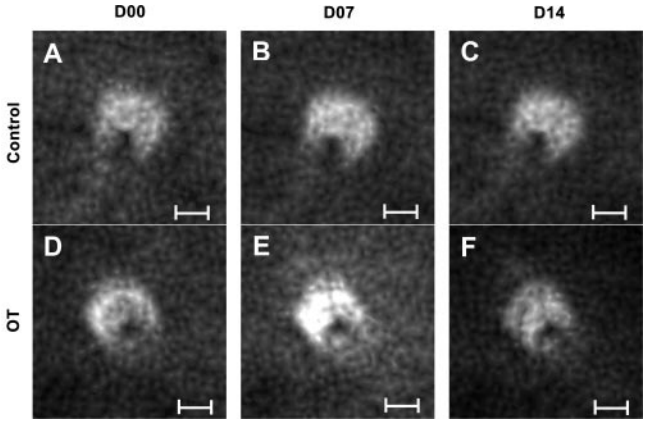

Figure 4. Representative noninvasive longitudinal retinal imaging of transgenic GFAP-GFP mice (control vs. OT). OT was performed unilaterally on the right eyes of 8-week-old transgenic mice, and left eyes were maintained as controls. Mice were subject to preoperative retinal imaging on day 0, followed by postoperative imaging on days 7 and 14. Each image is a composite from a total of 45 raw images nonlinearly aligned and averaged using our algorithm. The FI pattern remained fairly constant on all three time points (**A–C**) in the control eye, whereas a significant increase was observed from days 0 to 7 (**D**, **E**) in the transected eye, followed by a decrease from days 7 to 14 (**E**, **F**). Scale bars, 100 μm.

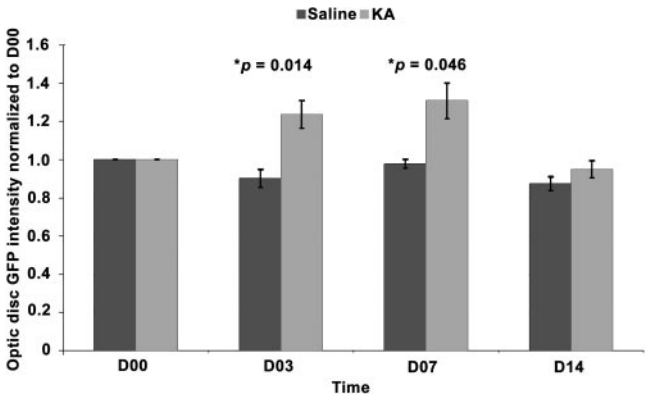

Figure 3. Quantification of fluorescent signal. FI for the optic disc astrocytes was measured from processed images of the saline and KA groups (n = 5), respectively. Measurements for day 0 were normalized to 1 as a reference for comparing the later longitudinal time points. A significant increase in FI for the retinas of KA-treated mice was observed on days 3 (P = 0.014) and 7 (P = 0.046). Quantified values were expressed as mean ± SEM and were statistically tested using the Friedman nonparametric comparison on repeated FI measures.

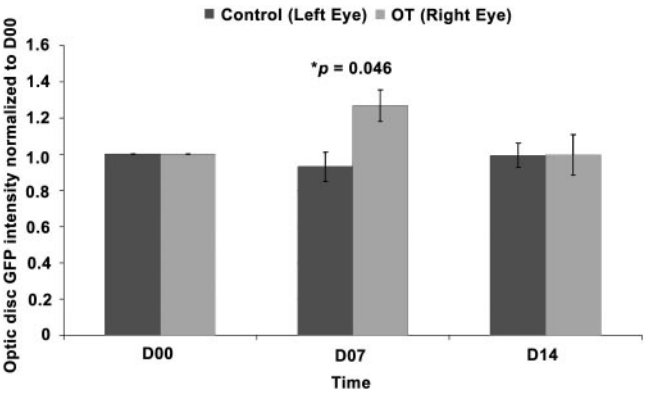

Figure 5. Quantification of fluorescent signal. FI for the optic disc astrocytes was measured from processed images of the control and the OT group (n = 4), respectively. Measurements for day 0 were normalized to 1 as a reference for comparing the later longitudinal time points. A significant increase in FI for the OT eyes was observed on day 7 (P = 0.046). Quantified values were expressed as mean ± SEM and were statistically tested using the Friedman nonparametric comparison on repeated FI measures.

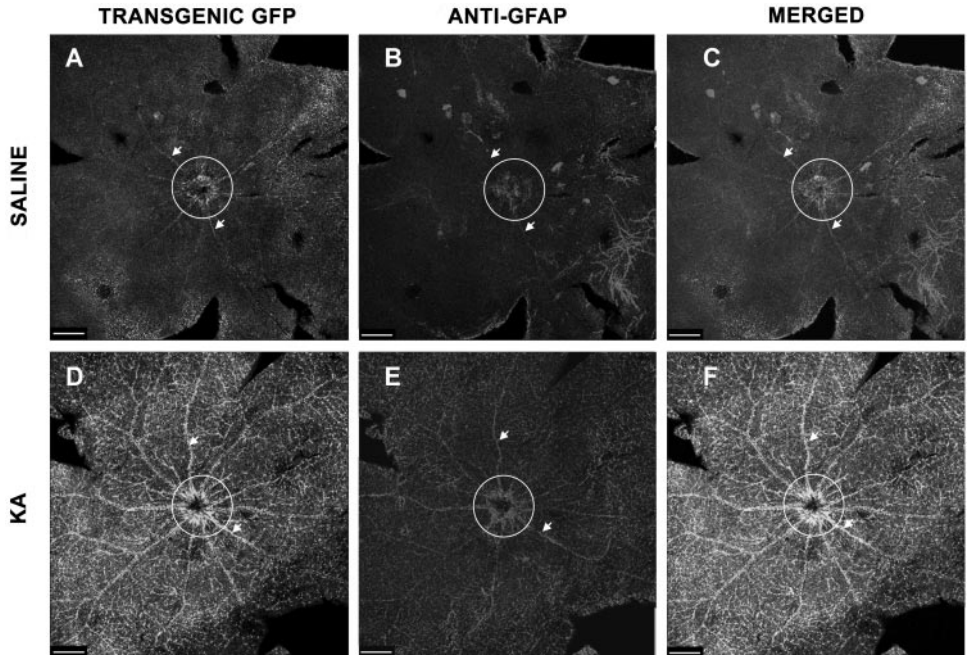

FIGURE 6. Representative double labeling of retinal wholemounts with GFP fluorescence and GAFP antibody. Retinal astrocytes on the optic disc (*circle*) and major blood vessels (*arrowheads*) at the NFL of a saline-treated transgenic mouse killed on day 7 were moderately labeled with GFP (**A**) and GFAP antibody (**B**), respectively. (**C**) Merged image of (**A**) and (**B**). Retinal astrocytes at the optic disc (*circle*) and major blood vessels (*arrowheads*) at the same layer of a KA-treated transgenic mouse killed on day 7 were intensely labeled with GFP (**D**) and GFAP antibody (**E**), respectively. (**F**) Merged image of (**D**) and (**E**). Scale bars, 200 μm.

puting software (MatLab; MathWorks) to be inadequate for detailed image analysis and GFP signal quantification at the cellular level. Therefore, we developed our own algorithm[33] to process and align multiple raw images as a solution to this problem. Averaging and denoising routines in our algorithm[33] effectively removed background noise such that the processed images indicate signal only from the retinal glial cells. It was clear from the processed images that the most intense fluorescence was from the retinal glia within the optic disc (Fig. 2). When temporally examined, the FI from the transgenic saline-treated retina remained fairly stable from day 0 through day 14 (Figs. 2A–D). On the contrary, the FI from the transgenic KA-treated retina showed a gradual increase of 24% ($P = 0.014$) at day 3 (Fig. 2F) and a maximum peak of 31% ($P = 0.046$) at day 7 (Fig. 2G), when P values were obtained using the Friedman nonparametric comparison on repeated FI measures. FI quantification ($n = 5$) for all time points was shown in Figure 3. The validity of our in vivo retinal imaging method was established by applying it to an OT mouse model known to cause retinal gliosis. Figure 4 shows a representative response of the OT eye, in which the FI peaks at day 7 and tapers back to normal by day 14. The quantified FI ($n = 4$) in Figure 5 confirms this observation, by which an increase of as much as 27% ($P = 0.046$) was shown on day 7. Conversely, the control eye is fairly constant for all three time points.

Retinal Wholemount IHC Confirms In Vivo Imaging on KA-Induced Gliosis

To verify that the noninvasively collected fluorescence signal was from the GFP in the retinal glia, we performed IHC on retinal wholemounts isolated from mice treated with KA or saline at day 7. Tiled confocal images of a low magnification show that both the endogenous GFAP and the transgenic GFP were expressed at a basal level in the retinal glia (astrocytes and Müller cells) in the saline control group (Figs. 6A–C). However, GFAP expression and GFP expression were significantly induced in the KA retina at day 7 (Figs. 6D–F). At a higher magnification (Fig. 7), hypertrophy and hyperplasia of retinal glia could be identified in the KA-treated retina (Fig. 7B). Figure 8 is a series of confocal images revealing retinal glia at various depths from the inner to the outer layer in the KA-treated and saline control retina. As expected, the retinal glia in

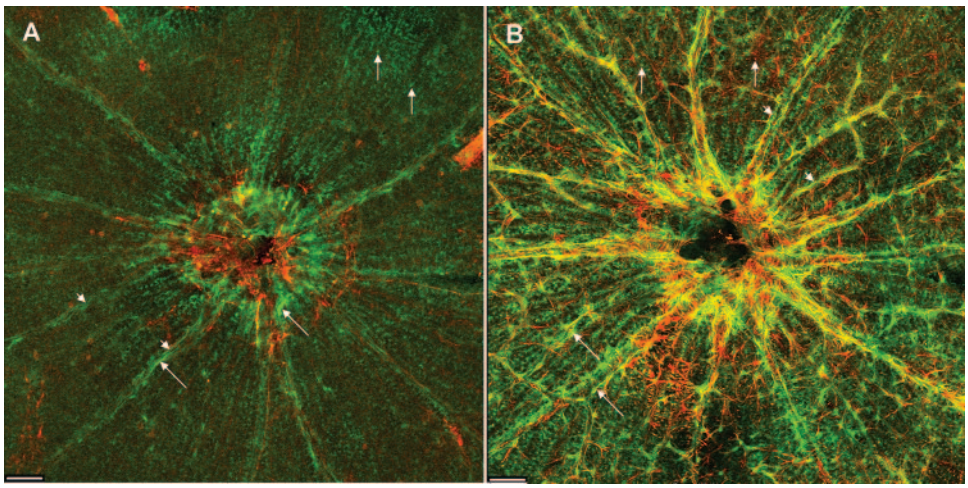

FIGURE 7. Higher magnification of the horizontal view at the NFL in retinal wholemounts. (**A**, **B**) Merged images of GFP (*green*) and GFAP (*red*) staining for saline and KA-treated retinas on day 7, respectively. Retinal vasculatures (*arrowheads*) were seen ensheathed by astrocytes (*long arrows*). Punctated spots (*short arrows*) of retinal glia are also visible in the retina surrounding the optic disc. It was obvious that GFP and GFAP staining for the KA-treated retina on day 7 were more intense, indicative of KA neurotoxicity. Scale bars, 50 μm.

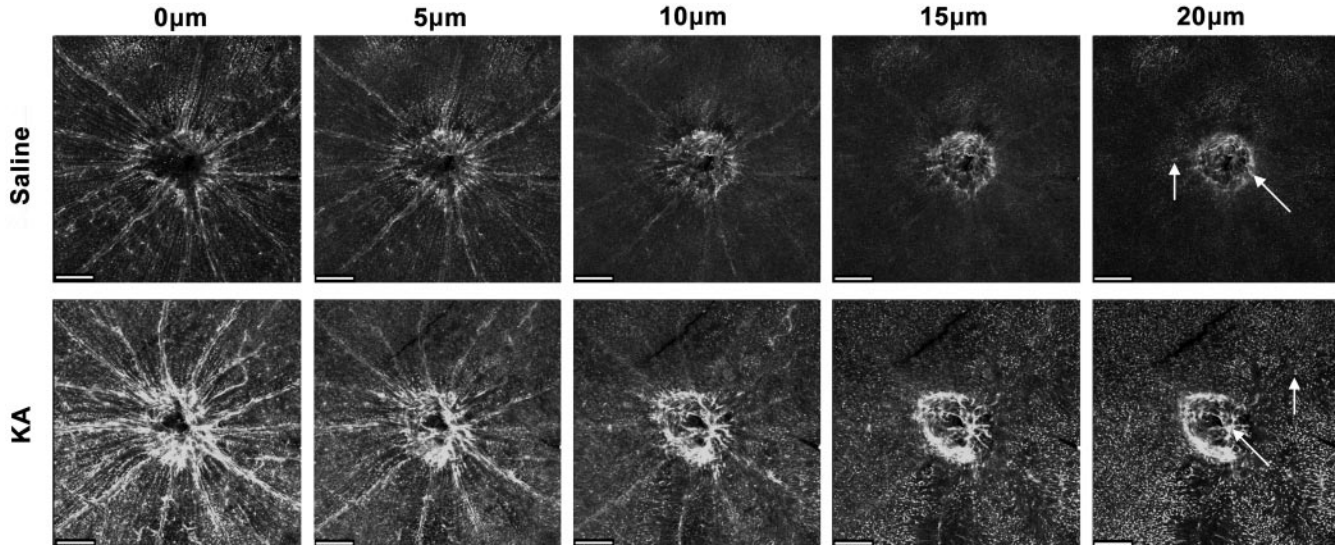

FIGURE 8. A serial *z*-axis view of confocal images focused at various depths (with 5-μm intervals) of the retinal wholemount, from the inner to the outer retina. At the depth of 0 μm (i.e., NFL), retinal glia is visible in the optic disc, around the blood vessels, and as punctate spots in the surrounding region. The depth from approximately 5 to 15 μm represented the ganglion cell layer, where astrocytic cell bodies were gradually disappearing. At the inner plexiform layer (15–20 μm), glia was visible mainly in the optic disc and surrounding region. In the saline-treated retina (*top row*), the GFP FI was at a basal level in both the optic disc (*long arrows*) and the surrounding regions (*short arrows*). In contrast, the GFP FI on day 7 was markedly induced by KA (*bottom row*) in both regions. Scale bars, 100 μm.

the KA-treated retina was highly activated compared with the saline control (Fig. 7A).

IHC Confirms KA-Induced Gliosis in the Hippocampus

IHC staining of the frozen brain section with the GFAP antibody (red) and the transgenic GFP (green) on the same focal plane clearly showed that KA induced severe and extensive reactive gliosis in the entire hippocampus (Figs. 9A, B), the localized areas of CA1 (Figs. 9C, D), CA3 (Figs. 9E, F), and dentate gyrus (Figs. 9G, H).

DISCUSSION

Seeliger et al.[31] and Paques et al.[32] reported that GFP under the control of smooth muscle α-actin promoter and chemokine fractalkine receptor CX_3CR1 promoter can be noninvasively detected from the retinal blood vessels and from the retinal microglia, respectively. However, no longitudinal or quantitative imaging was demonstrated in either study. To the best of our knowledge, the present report represents the first example of a real-time and quantitative study of retinal gliosis in living transgenic mice. We believe that it is possible to conduct a longitudinal and quantitative study of the mouse retina at a single cell resolution (Fig. 2) and to perform pattern recognition and analysis on the retinal glial network and vascular structure in health and disease by using our own algorithm.[33] However, this assertion remains to be tested with real data. The use of transgenic fluorescence for molecular retinal imaging with a scanning laser ophthalmoscope is unlikely to be translated to the clinical setting. Future development of nontoxic small molecular probes for a specific cellular target should open up the possibility of conducting molecular retinal imaging on humans.

Our noninvasive observation on retinal gliosis was consistent with previously published findings that documented an increase in GFAP in retinal glial cells after the administration of KA.[35,36] Hence, in the present study, we established a proof-

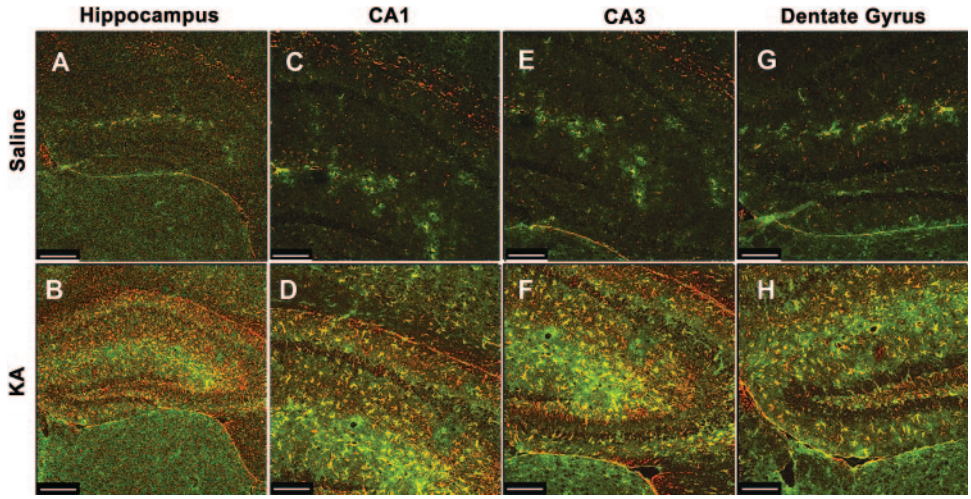

FIGURE 9. KA induced severe gliosis in multiple regions of the brain. At day 7, when the noninvasive retinal FI peaked (Fig. 2), severe gliosis could be seen in the entire hippocampus (**B**) compared with the saline-treated control (**A**). Similar results were observed in the hippocampal CA1 (**D**), CA3 (**F**), and dentate gyrus (**H**) compared with the saline-treated controls (**C**, **E**, **G**, respectively). Scale bars: (**A**, **B**) 200 μm; (**C**–**F**) 100 μm.

of-concept for using molecular retinal imaging to study retinopathies. Many neurodegenerative disorders, including Parkinson disease modeled after MPTP (Tsai JYY, et al. *IOVS* 2002;43:ARVO E-Abstract 1929), are accompanied by retinopathies and retinal gliosis in the central nervous system. Therefore, the molecular imaging described here can be used to investigate retinopathology during neurodegeneration. Finally, another useful application of the present method is to screen for compounds with neuroprotective properties in the transgenic mouse retina.

References

1. Wong TY, Shankar A, Klein R, Klein BEK, Hubbard LD. Prospective cohort study of retinal vessel diameters and risk of hypertension. *Br Med J.* 2004;329:79–83.
2. Hammond S, Wells JR, Marcus DM, Prisant LM. Ophthalmoscopic findings in malignant hypertension. *J Clin Hypertens.* 2006;8:221–223.
3. Topouzis F, Coleman AL, Harris A. Association of blood pressure status with the optic disk structure in non-glaucoma subjects: the Thessaloniki Eye Study. *Am J Ophthalmol.* 2006;142:60–67.
4. Mansour AM, Bitar FF, Traboulsi EI, et al. Ocular pathology in congenital heart disease. *Eye.* 2005;19:29–34.
5. Chan CC, Koch CA, Kaiser-Kupfer MI, et al. Loss of heterozygosity for the NF2 gene in retinal and optic nerve lesions of patients with neurofibromatosis 2. *J Pathol.* 2002;198:14–20.
6. Karadimas P, Hatzispasou E, Bouzas EA. Retinal vascular abnormalities in neurofibromatosis type 1. *J Neuro-Ophthalmol.* 2003;23:274–275.
7. Ruggieri M, Pavone P, Polizzi A, et al. Ophthalmological manifestations in segmental neurofibromatosis type 1. *Br J Ophthalmol.* 2004;88:1429–1433.
8. Antonetti DA, Barber AJ, Bronson SK, et al. Diabetic retinopathy: seeing beyond glucose-induced microvascular disease. *Diabetes.* 2006;55:2401–2411.
9. Takahashi H, Goto T, Shoji T, Tanito M, Park M, Chihara E. Diabetes-associated retinal nerve fiber damage evaluated with scanning laser polarimetry. *Am J Ophthalmol.* 2006;142:88–94.
10. Vujosevic S, Midena E, Pilotto E, Radin PP, Chiesa L, Cavarzeran F. Diabetic macular edema: correlation between microperimetry and optical coherence tomography findings. *Invest Ophthalmol Vis Sci.* 2006;47:3044–3051.
11. Onder C, Bengur T, Selcuk D, et al. Relationship between retinopathy and cirrhosis. *World J Gastroenterol.* 2005;11:2193–2196.
12. Kuhrt H, Walski M, Reichenbach A, Albrecht J. Rabbit retinal organ culture as an in-vitro model of hepatic retinopathy. *Graefe's Arch Clin Exp Ophthalmol.* 2004;242:512–522.
13. Guidry C, Medeiros NE, Curcio CA. Phenotypic variation of retinal pigment epithelium in age-related macular degeneration. *Invest Ophthalmol Vis Sci.* 2002;43:267–273.
14. Wang L, Cioffi GA, Cull G, Dong J, Fortune B. Immunohistologic evidence for retinal glial cell changes in human glaucoma. *Invest Ophthalmol Vis Sci.* 2002;43:1088–1094.
15. Helmlinger D, Yvert G, Picaud S, et al. Progressive retinal degeneration and dysfunction in R6 Huntington's disease mice. *Hum Mol Genet.* 2002;11:3351–3359.
16. Blanks JC, Schmidt SY, Torigoe Y, Porrello KV, Hinton DR, Blanks RH. Retinal pathology in Alzheimer's disease, II: regional neuron loss and glial changes in GCL. *Neurobiol Aging.* 1996;17:385–395.
17. Bruce EC, Andrew CP, Pentti TJ, David FB. Optic disc imaging in conscious rats and mice. *Invest Ophthalmol Vis Sci.* 2003;44:160–163.
18. Hawes NL, Smith RS, Chang B, Davisson M, Heckenlively JR, John SWM. Mouse fundus photography and angiography: a catalogue of normal and mutant phenotypes. *Mol Vis.* 1999;5:22–29.
19. Ritter MR, Aguilar E, Banin E, Scheppke L, Uusitalo-Jarvinen H, Friedlander M. Three-dimensional in vivo imaging of the mouse intraocular vasculature during development and disease. *Invest Ophthalmol Vis Sci.* 2005;46:3021–3026.
20. Dyer MA, Cepko CL. Control of Müller glial cell proliferation and activation following retinal injury. *Nat Neurosci.* 2000;3:873–880.
21. Kuzmanovic M, Dudley VJ, Sarthy VP. GFAP promoter drives Müller cell-specific expression in transgenic mice. *Invest Ophthalmol Vis Sci.* 2003;44:3606–3613.
22. Brenner M, Kisseberth WC, Su Y, Besnard F, Messing A. GFAP promoter directs astrocyte-specific expression in transgenic mice. *J Neurosci.* 1994;14:1030–1037.
23. Cordeiro MF, Guo L, Luong V, et al. Real-time imaging of single nerve cell apoptosis in retinal neurodegeneration. *Proc Natl Acad Sci U S A.* 2004;101:13352–13356.
24. Morgan J, Huckfeldt R, Wong RO. Imaging techniques in retinal research. *Exp Eye Res.* 2005;80:297–306.
25. Zhuo L, Sun B, Zhang CL, Fine A, Chiu SY, Messing A. Live astrocytes visualized by green fluorescent protein in transgenic mice. *Dev Biol.* 1997;187:36–42.
26. Genevois O, Paques M, Simonutti M, et al. Microvascular remodeling after occlusion-recanalization of a branch retinal vein in rats. *Invest Ophthalmol Vis Sci.* 2004;45:594–600.
27. Khoobehi B, Peyman GA. Fluorescent labeling of blood cells for evaluation of retinal and choroidal circulation. *Ophthalmic Surg Lasers.* 1999;30:140–145.
28. Hossain P, Liversidge J, Cree MJ, et al. In vivo cell tracking by scanning laser ophthalmoscopy: quantification of leukocyte kinetics. *Invest Ophthalmol Vis Sci.* 1998;39:1879–1887.
29. Jaissle GB, May CA, Reinhard J, et al. Evaluation of the rhodopsin knockout mouse as a model of pure cone function. *Invest Ophthalmol Vis Sci.* 2001;42:506–513.
30. Xu H, Manivannan A, Liversidge J, Sharp PF, Forrester JV, Crane IJ. Requirements for passage of T lymphocytes across non-inflamed retinal microvessels. *J Neuroimmunol.* 2003;142:47–57.
31. Seeliger MW, Beck SC, Pereyra-Munoz N, Dangel S, Tsai JY, Luhmann FO. In vivo confocal imaging of the retina in animal models using scanning laser ophthalmoscopy. *Vis Res.* 2005;45:3512–3519.
32. Paques M, Simonutti M, Roux MJ, et al. High resolution fundus imaging by confocal scanning laser ophthalmoscopy in the mouse. *Vis Res.* 2006;46:1336–1345.
33. Kumar S, Ho G, Zhuo L. Non-linear motion compensation for automated frame averaging of noisy in vivo images acquired from the retinas of transgenic GFP mice. *Opt Expr.* 2008;16:8250–8262.
34. Franklin KBJ, Paxinos G. *The Mouse Brain in Stereotaxic Coordinates.* 2nd ed. London: Academic Press; 2001.
35. Honjo M, Tanihara H, Kido N, Inatani M, Okazaki K, Honda Y. Expression of ciliary neurotrophic factor activated by retinal Müller cells in eyes with NMDA-and kainic acid-induced neuronal death. *Invest Ophthalmol Vis Sci.* 2000;41:552–560.
36. Sahel JA, Albert DM, Lessell S, Adler H, McGee TL, Konrad-Rastegar J. Mitogenic effects of excitatory amino acids in the adult rat retina. *Exp Eye Res.* 1991;53:657–664.